AMERICAN SOCIETY FOR MICROBIOLOGY | Journal of Bacteriology®

RESEARCH ARTICLE

Characterization of Engineered PreQ1 Riboswitches for Inducible Gene Regulation in Mycobacteria

Erik R. Van Vlack,[a] Shana Topp,[b]* Jessica C. Seeliger[c]

Department of Chemistry, Stony Brook University, Stony Brook, New York, USA[a]; Department of Chemistry, University of California, Berkeley, California, USA[b]; Department of Pharmacological Sciences, Stony Brook University, Stony Brook, New York, USA[c]

ABSTRACT We report here the behavior of naturally occurring and rationally engineered preQ1 riboswitches and their application to inducible gene regulation in mycobacteria. Because mycobacteria lack preQ1 biosynthetic genes, we hypothesized that preQ1 could be used as an exogenous nonmetabolite ligand to control riboswitches in mycobacteria. Selected naturally occurring preQ1 riboswitches were assayed and successfully drove preQ1-dependent repression of a green fluorescent protein reporter in *Mycobacterium smegmatis*. Using structure-based design, we engineered three preQ1 riboswitches from *Thermoanaerobacter tencongensis*, *Bacillus subtilis*, and *Lactobacillus rhamnosus* toward achieving higher response ratios and increased repression. Assuming a steady-state model, variants of the *T. tencongensis* riboswitch most closely followed the predicted trends. Unexpectedly, the preQ1 dose response was best described by a model with a second, independent preQ1 binding site. This behavior was general to the preQ1 riboswitch family, since the wild type and rationally designed mutants of riboswitches from all three bacteria behaved analogously. Across all variants, the response ratios, which describe expression in the absence versus the presence of preQ1, ranged from <2 to ~10, but repression in all cases was incomplete up to 1 mM preQ1. By reducing the transcript expression level, we obtained a preQ1 riboswitch variant appropriate for inducible knockdown applications. We further showed that the preQ1 response is reversible, is titratable, and can be used to control protein expression in mycobacteria within infected macrophages. By engineering naturally occurring preQ1 riboswitches, we have not only extended the tools available for inducible gene regulation in mycobacteria but also uncovered new behavior of these riboswitches.

IMPORTANCE Riboswitches are elements found in noncoding regions of mRNA that regulate gene expression, typically in response to an endogenous metabolite. Riboswitches have emerged as important tools for inducible gene expression in diverse organisms. We noted that mycobacteria lack the biosynthesis genes for preQ1, a ligand for riboswitches from diverse bacteria. Predicting that preQ1 is not present in mycobacteria, we showed that it controls optimized riboswitches appropriate for gene knockdown applications. Further, the riboswitch response is subject to a second independent preQ1 binding event that has not been previously documented. By engineering naturally occurring riboswitches, we have uncovered a new behavior, with implications for riboswitch function in its native context, and extended the tools available for inducible gene regulation in mycobacteria.

KEYWORDS inducible gene regulation, mycobacteria, preQ1, riboswitch

Received 7 September 2016 **Accepted** 3 January 2017

Accepted manuscript posted online 9 January 2017

Citation Van Vlack ER, Topp S, Seeliger JC. 2017. Characterization of engineered preQ1 riboswitches for inducible gene regulation in mycobacteria. J Bacteriol 199:e00656-16. https://doi.org/10.1128/JB.00656-16.

Editor Tina M. Henkin, Ohio State University

Address correspondence to Jessica C. Seeliger, jessica.seeliger@stonybrook.edu.

* Present address: Shana Topp, The Boston Consulting Group, Atlanta, Georgia, USA.

Riboswitches have emerged as important tools for inducible gene expression in diverse organisms. They are regulatory elements found in noncoding regions of mRNA that typically comprise on the order of 100 to 200 nucleotides (nt) in the 5′

untranslated regions (5′ UTRs) of bacterial genes involved in metabolite synthesis and regulate expression in response to an intermediate or product of the pathway. Both naturally occurring riboswitches and synthetic engineered riboswitches have been manipulated or created to provide a range of inducible responses in hosts from bacteria to mammals (recently reviewed in reference 1). Riboswitches have significant potential in a range of applications due to their portability and ease of manipulation by standard molecular biological methods. Their use in particular applications, such as gene silencing, metabolic engineering, and overexpression, often requires the optimization of characteristics such as tight control, dynamic range, and ligand responsiveness. Strategies to engineer riboswitches for such uses have included the creation of novel ligand-aptamer pairs, either *de novo* (starting from aptamers for synthetic ligands) or by engineering existing riboswitches for selective binding to a structurally related ligand, and by modulating the behavior of existing ligand-aptamer pairs.

Rational design, library selection/screening, or the two approaches in combination have led to moderately selective and, in several cases, extremely stringent ligand-dependent control. For example, synthetic theophylline-responsive riboswitches have been engineered to provide stringent gene control in diverse bacterial species, including *Acinetobacter*, *Francisella*, and *Mycobacterium* spp., for which few robust tools for regulated gene expression exist (2–4). For pathogenic *Francisella novicida* and *Mycobacterium tuberculosis*, inducible gene regulation was also demonstrated in bacteria within macrophages. The millimolar theophylline concentrations required are, however, moderately toxic to mammalian cells over the treatment period, and thus this limits their use in infection models, a compelling application for which only one tool, the Tet-inducible system (5), is currently available for mycobacteria.

As an alternative to *de novo* synthetic switches, naturally occurring riboswitches offer certain potential advantages since they already possess a highly selective, high-affinity aptamer coupled productively to an expression platform. However, because naturally occurring switches respond to endogenous metabolites, in order to serve as inducible gene regulation tools, they must be engineered to discriminate against the native metabolite and recognize instead an orthogonal, nonnatural ligand. Several studies have yielded riboswitches that bind to new ligands and retain switching behavior with moderate dynamic range (6–9).

In considering modifying naturally occurring riboswitches, we noted that mycobacteria lack the genes necessary to make preQ1, the ligand for riboswitches found in diverse bacteria but not mycobacteria. PreQ1 is a precursor to queuosine, a hypermodified nucleoside that is incorporated at the wobble position of His-, Asp-, Asn-, and Tyr-tRNAs and that modulates translational fidelity, likely by reducing frameshift errors (10). PreQ1 riboswitches are typically found in the 5′ untranslated regions (5′ UTRs) of genes related to queuosine biosynthesis. These riboswitches are classified into three classes and two subtypes based on sequence conservation and include examples of both transcriptional and translational control mechanisms (11). They have been extensively characterized *in vitro* for ligand binding and structure: They bind preQ1 with micromolar to nanomolar affinity and with high selectivity against structurally related metabolites, such as guanine, and they fold to form a core domain in the form of an H-type pseudoknot in which preQ1 is bound centrally at the junction between multiple stems (11, 12). In translationally controlled switches, preQ1-dependent repression is achieved via the sequestration of the ribosome binding site (RBS) in pairing interactions that form part of a stem. In transcriptionally controlled switches, preQ1 binding disrupts the formation of an antiterminator hairpin and permits the formation of a terminator hairpin, leading to preQ1-dependent transcription termination.

In queuosine biosynthesis, GTP is transformed into preQ1 by a series of four enzymes: QueD (EC 4.1.2.50), QueE (EC 4.3.99.3), QueC (EC 6.3.4.20), and QueF (EC 1.7.1.13) (13). Based on the protein sequences from *Escherichia coli*, QueF homologues are absent from mycobacteria. QueD (25 to 60% sequence identity), QueE (~30 to 35% identity), and QueC homologues (~30 to 40% identity) are annotated in several fast-growing mycobacteria and one sequenced sputum isolate of *M. tuberculosis* but

none of the virulent *M. tuberculosis* laboratory strains, such as H37Rv or the frequently studied nonpathogenic *M. smegmatis*. Based on this analysis, we predicted that preQ1 is not present and could therefore function as an orthogonal ligand to regulate riboswitches within most mycobacteria.

Our overall goal was to characterize the behavior and determine the applicability of preQ1 riboswitches for inducible gene knockdown. Our strategy was to assay first naturally occurring riboswitches using a green fluorescent protein (GFP) reporter system. We have previously determined that fast-growing nonpathogenic *M. smegmatis* is an appropriate host in which to characterize and optimize riboswitches for application to other mycobacteria such as *M. tuberculosis* (4). PreQ1 riboswitches representing different classes and types responded reversibly and in a dose-dependent manner in preQ1-treated bacteria, but the degree of repression would provide a highly limited dynamic range for knockdowns. We went on to modify several translationally controlled switches using structure-based design and based on the assumption that riboswitch function is dominated by thermodynamic factors. The rationally designed variants of the *T. tencongensis* riboswitch most closely followed predicted trends for changes in behavior upon mutation and yielded variants with the highest response ratios.

In the course of characterizing the preQ1 dose response, a second preQ1-dependent transition was detected at high micromolar to millimolar concentrations and, based on modeling, represented a second, independent binding event. These results showed that the dynamic range of the switches was greater and therefore more useful for gene regulation applications, than indicated by our preliminary characterization. Furthermore, this behavior has not been previously documented, likely because other studies were largely limited to observations at tens of micromolar preQ1.

By creating a vector that expressed lower levels of riboswitch-containing transcripts, we obtained a preQ1 riboswitch construct that significantly repressed protein expression for GFP and the mycobacterial protein LprG. This optimized riboswitch also controlled the expression of chromosomally encoded catalase-peroxidase KatG, which resulted in preQ1-dependent isoniazid resistance and indicated successful regulation of the relevant protein function. Finally, preQ1 repressed reporter gene expression reversibly in both nonpathogenic and pathogenic mycobacteria. The response was titratable in culture and achieved within macrophages at nontoxic preQ1 concentrations. These results demonstrated the utility of these switches for bacterial gene regulation both *in vitro* and in a cell-based model of infection. In summary, we successfully modified naturally occurring preQ1 riboswitches for inducible gene knockdown applications in mycobacteria and, in the course of doing so, discovered novel behavior for these riboswitches.

RESULTS

The preQ1 riboswitch family induces ligand dose-dependent gene repression in *M. smegmatis*. A panel of naturally occurring preQ1 riboswitches was tested for the ability to regulate GFP expression in *M. smegmatis* in response to preQ1. Expression was driven by a mycobacterial constitutive reporter (P_{hsp60}) (14) fused to a predicted or characterized riboswitch sequence (see Table S1 in the supplemental material). Each riboswitch was inserted 4 nt downstream of the P_{hsp60} transcriptional start site. Inserted sequences included the aptamer as reported and the downstream sequence through the start codon of the native gene locus. The selected riboswitches represent a cross-section of the reported classes (classes I, II, and III), types (types I and II) and predicted mechanisms (transcriptional or translational) (Fig. 1) (11, 15–17).

The resulting GFP reporter constructs in *M. smegmatis* displayed diverse responses to exogenous preQ1 in an endpoint fluorescence assay (Fig. 1). In all cases, repression was observed in the presence of preQ1, a finding consistent with our predictions and previous studies (6, 15). Initial dose-response and kinetics experiments on riboswitches from *B. subtilis* and *T. tencongensis* indicated saturating behavior at $\geq$100 μM preQ1 after 6 h (see Fig. S1 and S2 in the supplemental material). The response ratio was thus

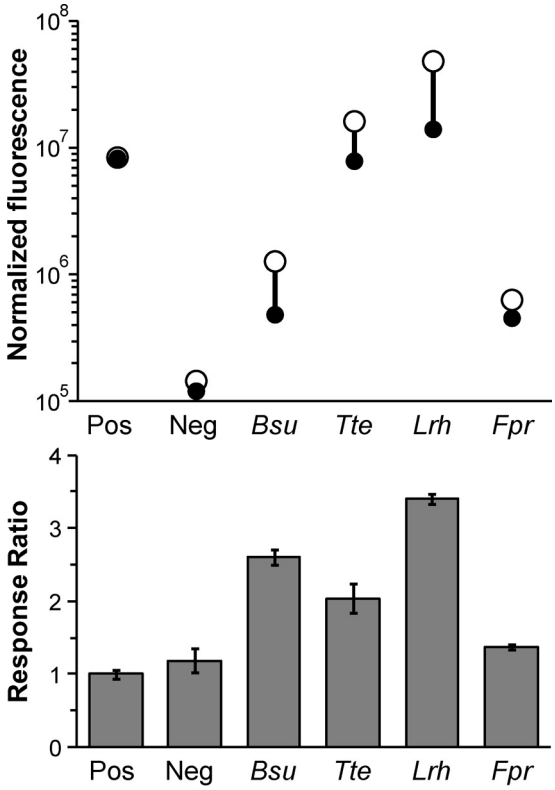

FIG 1 The preQ1 riboswitch family regulates ligand-dependent gene repression in *M. smegmatis*. (Top) GFP fluorescence normalized to OD_{595} in *M. smegmatis* whole cells in response to 0 μM (○) or 100 μM (●) preQ1 after 6 h (~2 doubling times). In all constructs transcription is driven by the P_{hsp60} promoter; the positive control (Pos) lacks the riboswitch, and the negative control (Neg) is empty vector. (Bottom) The response ratio for each riboswitch is F(0 μM)/F(100 μM), where F is the normalized fluorescence. Data are presented as means ± the standard errors of the mean (SEM) for at least three biological replicates.

defined as the GFP fluorescence normalized to the cell density (i.e., the optical density at 595 nm [OD_{595}] at 0 μM preQ1 versus that at 100 μM preQ1). Across the five naturally occurring riboswitches tested, response ratios ranged from 1.3 to 3.7 (Fig. 1). Although the range of response ratios was narrow, the choice of riboswitch significantly influenced both the maximum observed fluorescence in the absence of preQ1 and the minimum fluorescence at 100 μM preQ1; these varied between different riboswitches over a range of ~75- to ~30-fold, respectively. Notably, GFP expression was not fully repressed at 100 μM preQ1 for any riboswitch or up to 1 mM preQ1 for the *T. tencongensis* and *L. rhamnosus* riboswitches (see Fig. 4B and D). To test whether active efflux of preQ1 influences observed riboswitch responses by limiting intracellular preQ1, cells were incubated with the efflux pump inhibitors carbonyl cyanide 3-chlorophenylhydrazone (CCCP) or reserpine simultaneous with preQ1 treatment. No effect on the preQ1 dose response was observed with either inhibitor (see Fig. S3 in the supplemental material).

Stabilization of the OFF state leads to increased repression in the *T. tencongensis* riboswitch. After reviewing the panel of naturally occurring riboswitches, we hypothesized that increasing the thermodynamic stability of the repressive conformation of the riboswitch would increase the response ratio, based on a steady-state model with two states, ON and OFF, represented by the conformations A and B (see Fig. 4A, scheme 1). Our aim was to stabilize the OFF state selectively in the presence of ligand, although in general stabilizing mutations are likely to reduce expression in both the presence and the absence of preQ1. We started with the *T. tencongensis* riboswitch because it displayed GFP expression levels that would provide sufficient dynamic range to characterize the broad range of effects likely to be introduced by mutation (Fig. 1).

Also, the wealth of available biochemical, biophysical, and structural information facilitated the design of mutations that would test our assumption that switching behavior is dominated by the equilibrium between the ON and OFF states and therefore can be engineered rationally by modulating their relative free energies.

Based on the crystal structures of the *T. tencongensis* riboswitch (17), we created a series of insertion mutations designed to introduce additional pairing interactions with the putative RBS while, ideally, preserving the core aptamer structure and ligand affinity. To achieve this, 8 to 15 nt were inserted between G8 and C9 to create 11 *T. tencongensis* riboswitch variants (T1 to T11) (Fig. 2A). For each insertion, approximately half of the inserted nucleotides were chosen to pair with various degrees of affinity with the RBS (using either Watson-Crick or wobble interactions) and thereby extend the P2 stem. The remaining nucleotides were noncomplementary to any neighboring sequence and were intended to provide an unstructured loop connecting the P2 stem back to aptamer at G8 and thereby minimize perturbation to the core aptamer structure (Fig. 2A). Due to the difficulty in predicting the folding and free energy of pseudoknots, free energies were calculated only for the stem by itself (see Materials and Methods). Assuming that the chosen changes do not destabilize the aptamer, the longer stems formed by these insertions were predicted to lower the free energy by 3 to 14 kcal mol^{-1} (18). The range of energies was chosen based on the results of Mishler and Gallivan (19), who showed that changes of ~1 kcal mol^{-1} in the stability of the sequester helix of an artificial theophylline riboswitch altered the response ratio in *E. coli* by 2- to 10-fold.

GFP expression driven by *T. tencongensis* variants T1 to T11 was assayed, and the response ratios were determined in the fluorescence endpoint assay. For the *T. tencongensis* variants, the observed trend in the fluorescence maxima and minima and the response ratios followed predicted trends qualitatively, based on the relative free energies of the extended P2 stem: the greater the predicted stability of the OFF state, the higher the response ratio (variants T1 through T4) (Fig. 2B). The T4 variant displayed the highest response ratio of ~8. In comparison, GFP expression driven by the TetR system was 2-fold lower than T4 under permissive conditions (200 ng/ml anhydrotetracycline inducer) but ~4-fold lower under repressive conditions (0 ng/ml anhydrotetracycline), resulting in a 2-fold higher response ratio. Overall, across the *T. tencongensis* variants, a higher response ratio was achieved at the cost of maximum expression and therefore the overall range of expression (−preQ1) (Fig. 2B, open circles) and as a result of the arithmetic artifact of dividing by increasingly lower values for minimum expression (+preQ1) (Fig. 2B, filled circles). Indeed, as predicted stability increased across variants T7 through T11, expression became nearly independent of preQ1. Even so, repression was still incomplete for all variants at 100 μM preQ1, since fluorescence in all cases was greater than for that of the negative vector control.

Up to severalfold higher expression in the absence of preQ1 was observed for variants T1 to T3 compared to the wild type, suggesting that in addition to introducing stabilizing interactions, the insertion of a loop proximal to P2 also had destabilizing effects that favor the ON state. Therefore, a control variant (T1*) was created in which 8 nt that are noncomplementary to any proximal sequence were inserted between G8 and G9. However, T1* did not display significant switching behavior and did not recapitulate the elevated GFP expression observed for variant T1 compared to the wild type (Fig. 2B).

PreQ1 riboswitches representing other types and classes diverge from the class I type II *T. tencongensis* riboswitch in response to mutation. We hypothesized that analogous engineering principles could be applied to related riboswitches such as the *B. subtilis* switch, a type I class I preQ1 riboswitch. In the *B. subtilis* switch, the expression platform involves terminator/antiterminator hairpins that regulate transcription (15). Since the rational modification of transcriptional regulation is not immediately intuitive, in order to facilitate our design efforts, we first tested whether the switch would tolerate modification to a translational mechanism. We noted that the 3′ end of the ligand-bound structure includes base-pairing interactions with a sequence rich in A

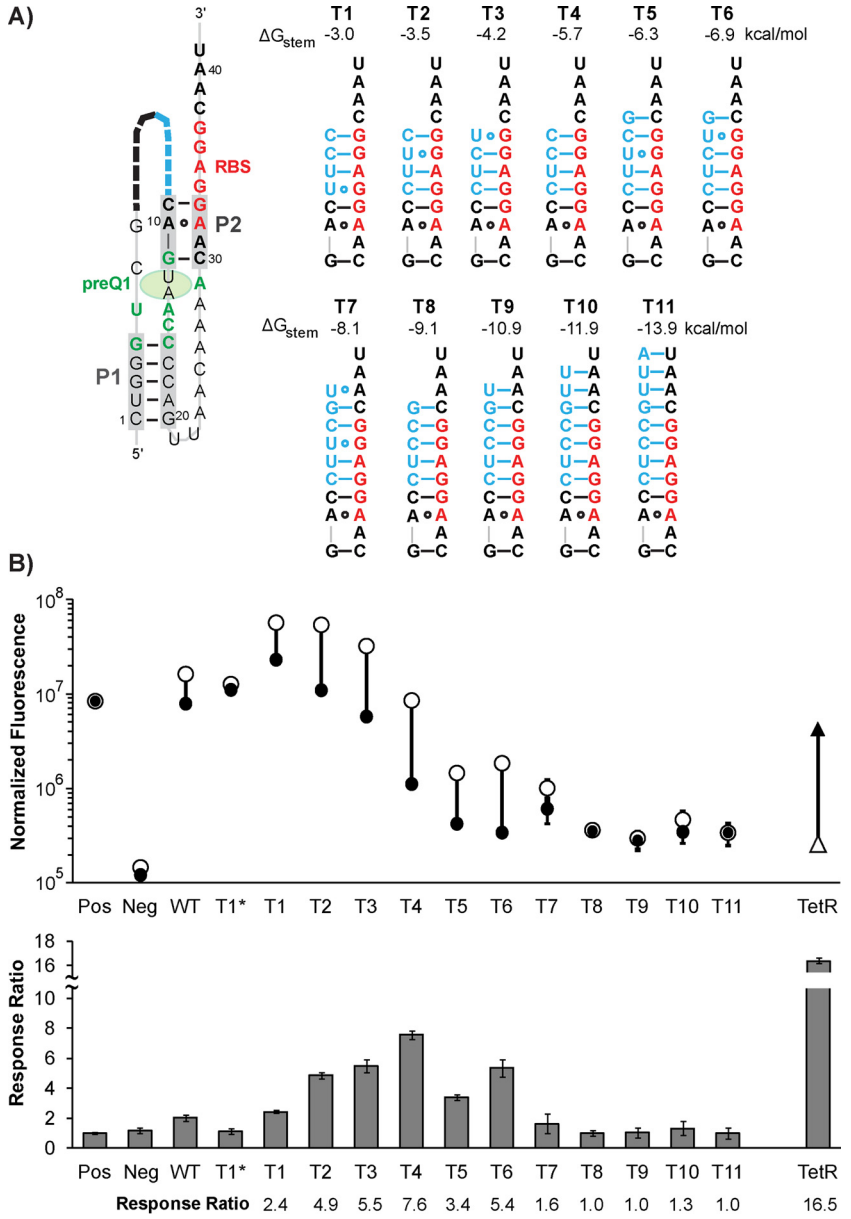

FIG 2 The responses of *T. tencongensis* riboswitch variants to preQ1 correlate with thermodynamic predictions. (A) Diagram of the *T. tencongensis* riboswitch with the inserted sequence introduced by mutation shown as a dashed line. Also highlighted are nucleotides that make key interactions with preQ1 (green) and that form the putative RBS (red). Shown at right are the stem structures predicted upon mutation. The specified sequence (blue) was inserted between G8 and C9 (numbering as previously published [22]). The Δ*G* of each stem was calculated with mfold by connecting G11 and C30 with an A_6 linker. The wild-type P2 stem was insufficiently stable to obtain a predicted Δ*G*. (B, top) GFP fluorescence normalized to an OD_{595} in *M. smegmatis* whole cells after 6 h (~2 doubling times) in response to 0 μM (○) or 100 μM (●) preQ1. Data for the TetR system are shown as in response to 0-ng/ml (△) or 50-ng/ml (108 nM; ▲) anhydrotetracycline. (Bottom) Response ratios calculated from the fluorescence data. Controls (Pos and Neg) are the same as for Fig. 1. Data are presented as means ± the SEM for at least three biological replicates.

and G that resembles a conserved RBS and therefore suggested an avenue for engineering translational control, in direct analogy with naturally occurring translationally controlled preQ1 class I type II riboswitches such as the *T. tencongensis* riboswitch. In the variant *B. subtilis trans*, the wild-type riboswitch sequence was modified with a single C-to-G nucleotide substitution (Fig. 3A) to create a consensus prokaryotic RBS sequence (AGGAGG), followed by 10 nt and the start ATG codon for a GFP reporter

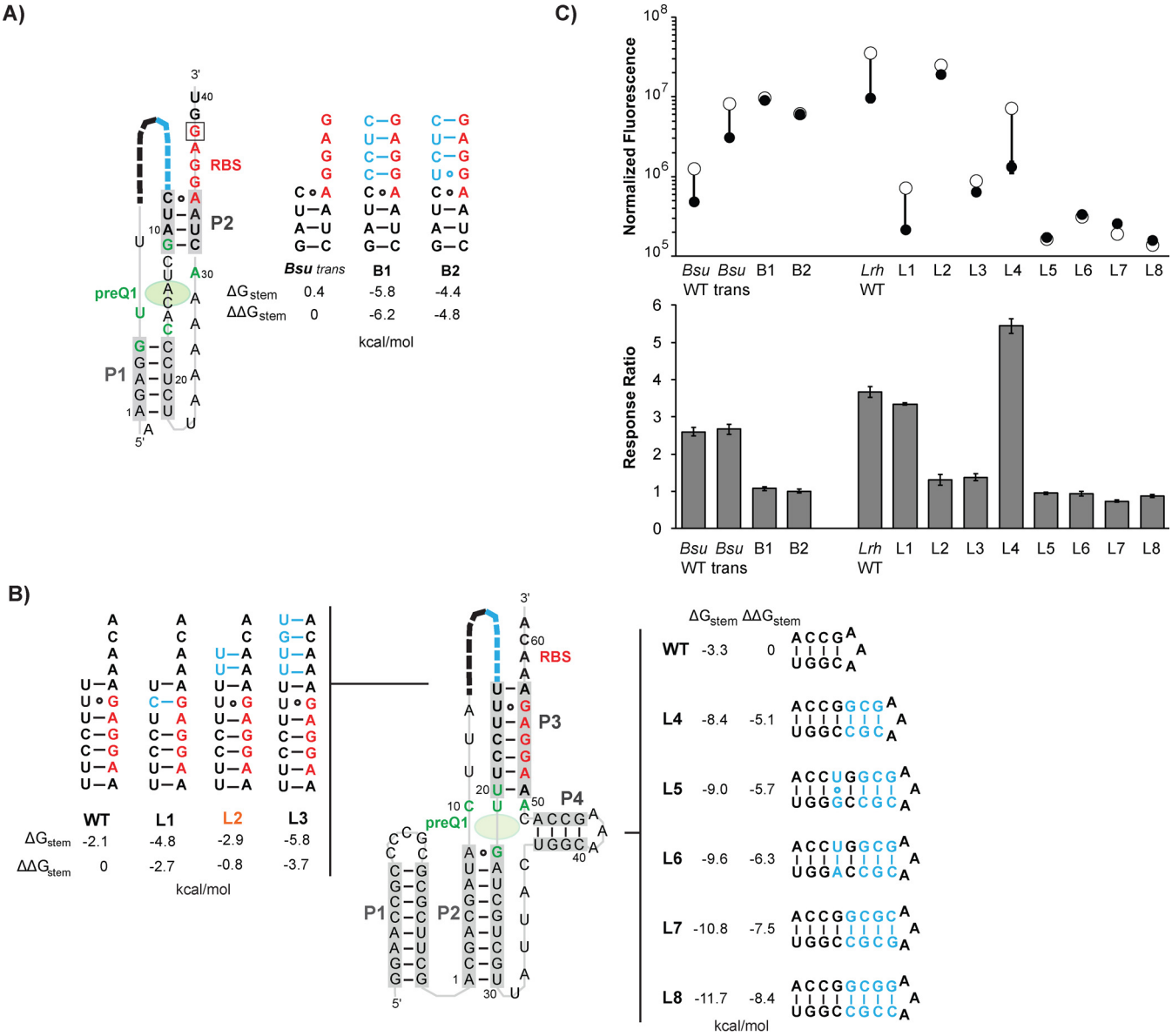

FIG 3 The responses of *B. subtilis* and *L. rhamnosus* riboswitch variants to preQ1 do not conform with thermodynamic predictions. (A) Diagram of the *B. subtilis trans* riboswitch. The C38G mutation used to create the *trans* variant is outlined by a box. (B) Diagram of the *L. rhamnosus* riboswitch. For both panels A and B, the inserted sequence introduced by mutation is indicated as a dashed line. The predicted stem structures are indicated with the inserted residues in blue. Also highlighted are nucleotides that make key interactions with preQ1 (green) and that form the putative RBS (red). The Δ*G* of each stem connected by A_6 linker was calculated with mfold; the Δ*G* of the P4 stem was calculated with the sequences shown. (B, top) GFP fluorescence normalized to an OD_{595} in *M. smegmatis* whole cells after 6 h in response to 0 μM (○) or 100 μM (●) preQ1. (Bottom) Response ratios calculated from the fluorescence data. Data are presented as means ± the SEM of at least three biological replicates.

gene. In *M. smegmatis* this construct had significantly higher GFP expression than the wild type both in the absence and in the presence of preQ1 and displayed a similar response ratio of ~2 (Fig. 3C). Thus, the *B. subtilis* switch was successfully transformed from a transcriptional to a translational regulatory mechanism.

Applying the same strategy as for the *T. tencongensis* riboswitch, insertion mutations were made in the *B. subtilis trans* riboswitch to extend the loop between P1 and P2 and thereby lengthen P2 (Fig. 3A). Variants B1 and B2 were designed to include stabilizing interactions and favor the OFF state. In the GFP endpoint assay both variants displayed higher expression relative to the parent switch in the absence of preQ1, but in contrast to predictions and in contrast to the *T. tencongensis* variants, they lost sensitivity to preQ1 and showed little to no ligand-dependent repression (Fig. 3C).

Given these contrasting results in related class I switches, we further tested the applicability of our design strategy by modifying the *L. rhamnosus* riboswitch, a class II preQ1 riboswitch with a modified structure that shares a pseudoknot architecture but has an additional stem-loop (P4) between P2 and P3 (Fig. 3B) (20). Working from the crystal structure, mutations were designed to stabilize the P3 stem with additional pairing interactions to the putative RBS by substitution (U35C) or by lengthening P3 by inserting nucleotides between U34 and U35 to yield variants L1 to L3. In addition, since *L. rhamnosus*-specific P4 is thought to stabilize the preQ1 binding site, we extended this stem by inserting additional Watson-Crick pairs (variants L4 to L8) (Fig. 3B) (21). GFP expression driven by the resulting *L. rhamnosus* variants L1-L8 was assayed, and the response ratios were determined in a fluorescence endpoint assay (Fig. 3C).

GFP expression was significantly reduced in variant L1, in which a single nucleotide substitution (U35C) changed a wobble (G-U) to a Watson-Crick (G-C) pair. Additional base pairing introduced near the RBS and downstream of U35 in variants L2 and L3 also lowered the response ratio and, in the case of variant L3, almost completely suppressed GFP expression. In contrast, extending P4 with three Watson-Crick pairs increased the response ratio to >5 for variant L4. However, introducing additional pairing interactions in variants L5 to L8 effectively precluded GFP expression independent of preQ1. Like the *B. subtilis trans* variants B1 and B2, these variants are presumably predominantly in the OFF state even in the absence of preQ1, and the switch is thus insensitive to preQ1, within the detection limits and reproducibility of the assay.

The dose response behavior of preQ1 riboswitches requires a steady-state model with two independent binding sites. Among all preQ1 riboswitch variants tested, the greatest response ratio observed was ~8 at 100 μM preQ1. Initial experiments had suggested that the response of wild-type switches was fully saturated at this concentration, and all measurements on riboswitch variants were made at this concentration on the assumption that the dissociation constant for preQ1 was not altered by mutation. Since preQ1 does not inhibit *M. smegmatis* growth at <5 mM (see Fig. S4 in the supplemental material), we tested this assumption by measuring the dose response over an extended concentration range up to 1 mM preQ1 for *T. tencongensis* variants T1 to T6, *B. subtilis trans* B1-B2, *L. rhamnosus* L2, and the corresponding parent riboswitches. Unexpectedly, most variants displayed a second repressive transition at higher preQ1 concentrations with an apparent half-maximal effective concentration (EC_{50}) of ~100 μM preQ1 (see Fig. 4B to D). This additional dose-dependent repression at high micromolar to millimolar preQ1 was also observed for the three parent riboswitches and is thus inherent to the riboswitch rather than due to mutation. Importantly, GFP expression driven by a constitutive promoter without a riboswitch was not significantly affected by up to 1 mM preQ1 (see Fig. S5 in the supplemental material). Therefore, the behavior is not due to the nonspecific effects of preQ1 on GFP expression or fluorescence.

Assuming the steady-state model, multiple independent transitions can only arise from multiple independent binding sites (Fig. 4A, scheme 2). The presence of additional ON or OFF states would shift the apparent K_d but would not lead to multiple transitions in the dose response. Incorporating a second, independent binding site into the model resulted in a more accurate fit to the observed data (Fig. 4B). Because concentrations of >2 mM preQ1 inhibited *M. smegmatis* growth, the response was not measured at these concentrations (see Fig. S4 in the supplemental material). The robustness of the fits was thus limited, especially for variants with low overall GFP expression (e.g., variants T5 and T6) (Fig. 4B). Nevertheless, general trends in K_{int} and K_{d1} across variants and approximate lower limits for K_{d2} could be determined (Table 1).

As predicted by the calculated free energies of the extended P2 stem (Fig. 2A) and corresponding stabilization of the OFF state, the observed K_{int} increased from variant T1 to T6. The dissociation constant K_{d1} was consistent across all variants T1 to T6, with an average value of 12 nM, similar to values for preQ1 binding reported *in vitro* (2 to 7 nM). In contrast, the wild-type *T. tencongensis* riboswitch had an apparent K_{d1} of ~100 nM, or 2 orders of magnitude weaker than the *in vitro* value for the aptamer, and an order

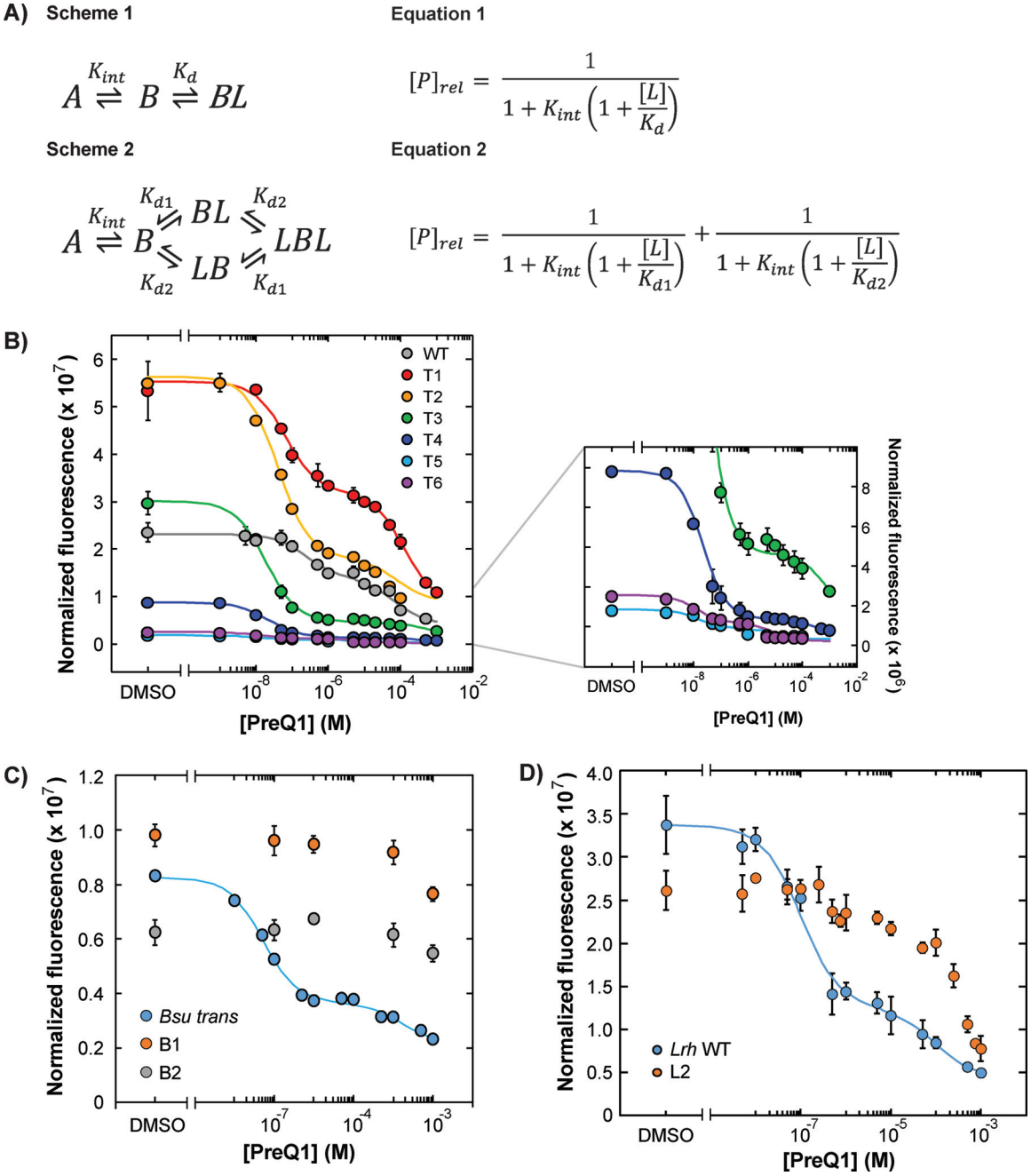

FIG 4 The dose response of preQ1 riboswitches is best described by a two-state model with two independent preQ1 binding sites. (A) A two-state model (scheme 1) based on the steady-state assumption in which the observed response, $[P]_{rel}$ (the relative protein concentration), as a function of ligand L is determined by K_{int} and K_d, which represent the equilibrium between the ON state (*A*) and the OFF state (*B* or *B* bound to *L*) and the dissociation constant for the aptamer (equation 1). In the case where the B state has two independent ligand-binding sites (scheme 2), the response depends on two dissociation constants, K_{d1} and K_{d2} (equation 2). (B to D) GFP fluorescence normalized to OD_{595} in *M. smegmatis* whole cells in response to various concentrations of preQ1 or DMSO vehicle after 6 h for the *T. tencongensis* (with a zoomed graph highlighting variants T3-T6 at right) (B), *B. subtilis trans* (C), and *L. rhamnosus* (D) riboswitches and selected variants. The data series for the wild-type riboswitches and *T. tencongensis* variants T1 to T6 were fit to equation S12 in the supplemental material (see Table 1). The data presented are means ± the SEM of technical triplicates from at least two biological replicates.

of magnitude greater than for the variants (Table 1). Fits for K_{d2} were less robust but were overall ~1,000-fold greater than K_{d1}, in the range of at least ~10 to 100 μM.

The *B. subtilis trans* riboswitch displayed similar biphasic behavior to that of the *T. tencongensis* riboswitch, (Fig. 4C; Table 1). Interestingly, in contrast to the wild-type *T. tencongensis* riboswitch, K_{d1} is on the same order as values reported *in vitro* for the *B.*

TABLE 1 Thermodynamic parameters for riboswitches based on a two-state model with two independent binding sites

Variant	K (μM)					$\Delta\Delta G$(T4)[b]	
	K_d (aptamer)[a]	K_{d1}	K_{d2}	K_{int}	ΔG (kcal mol^{-1})	K_{int}	mfold
T. tencongensis	0.002 (17), 0.007 (22)	0.1145	128	0.67	0.24	0.59	
T1		0.014	27	0.28	0.77	1.12	2.7
T2		0.015	29	0.59	0.31	0.66	2.2
T3		0.009	311	0.89	0.07	0.42	1.5
T4		0.014	113	1.79	−0.35	0	0
T5		0.011	9	3.52	−0.76	−0.41	−0.6
T6		0.009	6	2.53	−0.56	−0.21	−1.2
B. subtilis trans	~0.1 (17)	0.035	109	2.0			
L. rhamnosus	0.018 (22)	0.055	54	0.78			

[a]References are indicated in parentheses where applicable.
[b]$\Delta\Delta G$(T4) values are the values relative to T4 based on K_{int} or mfold calculations.

subtilis aptamer (Table 1) (15, 17, 22). However, variants B1 and B2 showed no response to preQ1 in the micromolar range, although a repressive trend was still apparent at high micromolar preQ1 to millimolar preQ1. Finally, the *L. rhamnosus* riboswitch and its variant L2 both displayed a preQ1 dose-dependent response at high micromolar preQ1 (Fig. 4D). This transition was especially pronounced in variant L2, which had little sensitivity to preQ1 below 100 μM. As a result, the response ratio for L2 was 1.3 when calculated using the fluorescence at 100 μM but increased to 3.3 when calculated using the fluorescence at 1 mM. Fitting the wild-type dose response to a model with two binding sites yielded a K_{d1} of ~6 nM and K_{d2} of ~54 μM. Thus, similar to the *B. subtilis trans* riboswitch, the apparent K_{d1} for the *L. rhamnosus* riboswitch is on the same order as the reported K_d of 18 nM for the aptamer *in vitro* (Table 1).

Lowering gene dosage improves the preQ1 riboswitch for inducible knockout applications. Of the riboswitch variants assayed, the *T. tencongensis* variants T3 and T4 (response ratios ~6 and ~8) showed the greatest promise for inducible gene regulation in mycobacteria. For inducible knockout applications, however, these variants were still inappropriate due to significant expression even in the presence of 1 mM preQ1 (Fig. 3B). We have previously observed for the theophylline riboswitch that lowering transcript levels (e.g., by changing the strength of the upstream promoter) reduces protein expression across the entire dose-response range and can thereby be used to modulate the response ratio in a manner independent of modulating the OFF state by mutation (23).

To test the effect of this additional design strategy on the preQ1 riboswitch, we lowered transcript levels by reducing the gene copy number from ~3 (using an episomal vector) (24) to 1 (using an integrating vector) and assayed the preQ1-dependent repression of not only GFP but also the mycobacterial protein LprG by immunoblotting. After 6 h of preQ1 treatment, GFP controlled by the T3 variant was still detectable by immunoblotting even at 1 mM preQ1 but was absent at both 0.1 and 1 mM preQ1 when regulated by the T4 riboswitch (Fig. 5A). These results were consistent with the fluorescence measurements of multicopy GFP, in which the T4 variant yielded lower expression in the absence of preQ1 and overall better repression (Fig. 2B). To test its general ability to repress protein expression, the T4 riboswitch was then applied to a single epitope-tagged copy of the mycobacterial protein LprG. After 6 h of preQ1 treatment, LprG levels were reduced by only a few fold even at 1 mM preQ1 (data not shown). To test whether longer treatment time would improve repression, cells were treated with preQ1 for 18 h, after which LprG was present at significantly reduced levels at all preQ1 concentrations tested, although still detectable at 1 mM (Fig. 5C). These results demonstrate that preQ1 riboswitches are broadly applicable, as shown by inducible repression of two proteins, and that the kinetics of repression can be target dependent, since LprG required significantly longer treatment time than GFP to achieve maximum repression under the conditions used.

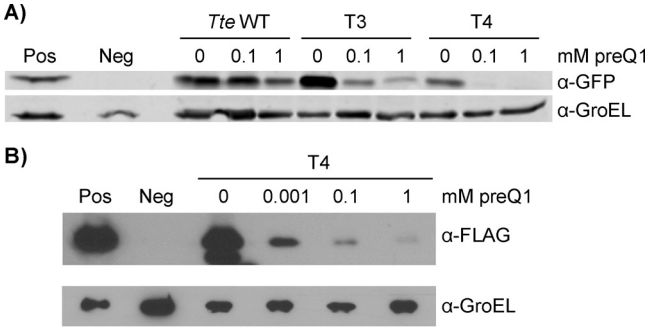

FIG 5 Proteins expressed from a single gene copy are repressed by the T4 riboswitch. (A) Immunoblot analysis of total lysates from *M. smegmatis* expressing GFP from a single integrated gene copy controlled by the *T. tencongensis* wild-type (WT) or T3 or T4 variant riboswitches after 6 h of incubation with DMSO vehicle or the indicated concentrations of preQ1. (B) Immunoblot analysis of total lysates from *M. smegmatis* expressing LprG from a single gene copy under the control of the T4 riboswitch after 18 h of incubation with the indicated concentrations of preQ1 or DMSO vehicle. For all immunoblots, the positive control (Pos) was the corresponding gene controlled by the *hsp60* constitutive promoter and the negative control (Neg) was empty vector. Sample loads were normalized to absorbance at 280 nm and GroEL was used a loading control. Data are representative of at least two clones or two biological replicates.

An optimized riboswitch enables preQ1-inducible antibiotic resistance via regulation of endogenous KatG expression. To test the T4 riboswitch for successful knockdown of an endogenous gene in a relevant functional assay, we generated by single crossover an *M. smegmatis* strain in which the gene encoding the catalase-peroxidase KatG was controlled by the T4 variant (Fig. 6A). The resulting recombinant strain, T4 RiboS-*katG*, displayed preQ1-dependent resistance to isoniazid, a prodrug that is activated by KatG (Fig. 6B). Isoniazid sensitivity similar to that of wild-type *M. smegmatis* was observed in the absence of preQ1, showing that *M. smegmatis* T4 RiboS-*katG* expresses sufficient KatG to support a wild-type level of function. Similarly, isoniazid resistance for T4 RiboS-*katG* under the most repressive conditions (1 mM preQ1) was similar to that for an analogous strain in which KatG expression is controlled by a synthetic theophylline riboswitch (EC_{50}s of 34 ± 9 and 21 ± 4 μg/ml, respectively) (4). These comparisons show that in this context both preQ1- and theophylline-inducible riboswitches yield phenotypically similar ranges of function.

PreQ1 riboswitches enable reversible and titratable expression both *in vitro* and in a cell-based model of infection. To further demonstrate the versatility of preQ1 riboswitches for inducible gene regulation in mycobacteria, we examined the

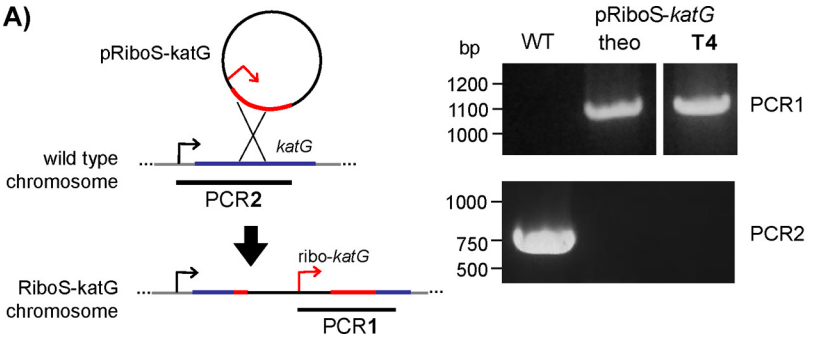

B)

	Isoniazid EC50 (μg/mL)	
[preQ1] (mM)	wild type	T4 RiboS-katG
0	5 ± 1	7 ± 3
0.1		16 ± 4
1	6 ± 1	34 ± 9

FIG 6 PreQ1 controls KatG-dependent sensitivity to isoniazid. (A) A single recombination event between the *M. smegmatis* chromosome and a suicide plasmid containing a promoter-riboswitch combination and 500 bp of *katG* yielded the T4 RiboS-*katG* strain containing a single full-length copy of *katG* under T4 riboswitch control. PCR1 probed for *katG* with an upstream riboswitch. As predicted, a 1,050-bp product is observed only for the recombinant strains T4 RiboS-*katG* or an analogous strain, theophylline-driven RiboS-*katG*, in which *katG* is controlled by a synthetic theophylline-inducible riboswitch (4). PCR2 probed for *katG* with an intact native upstream region. As predicted, an 850-bp product is observed only for the wild type (WT). All samples for PCR1 were run on the same gel; empty lanes were cropped for clarity. (B) The half-maximal effective concentration (EC_{50}) for isoniazid was measured for *M. smegmatis* as a function of preQ1 concentration. Dose-dependent EC_{50}s were observed for T4 RiboS-*katG* strain but not wild-type *M. smegmatis*. EC_{50} values are reported as the average of four replicates ± the standard deviations.

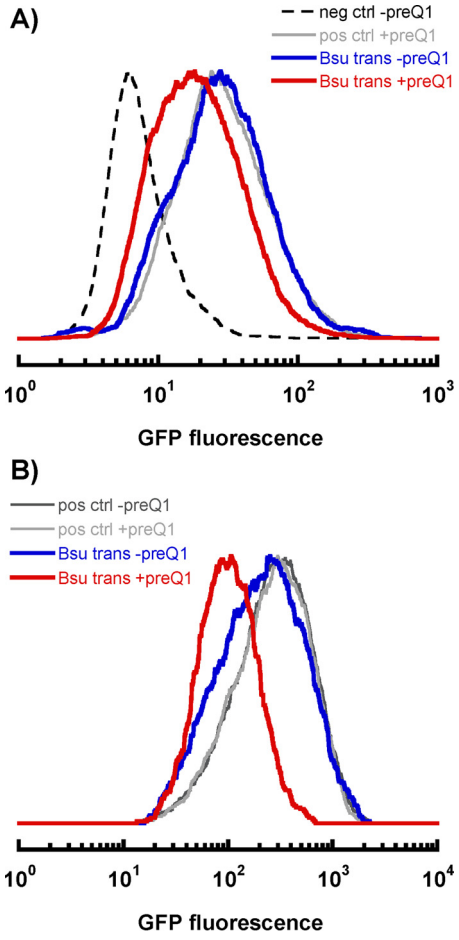

FIG 7 PreQ1 represses protein expression in mycobacteria within macrophages. (A) J774A.1 macrophage-like cells were infected with *M. smegmatis* harboring vector only (−ctrl) or GFP under the control of the *hsp60* constitutive promoter (+ctrl) or the *B. subtilis trans* riboswitch (*B. subtilis trans*). All strains also constitutively expressed mCherry as a live-cell marker. Infected cells were treated with DMSO vehicle (−preQ1) or 1 mM preQ1 (+preQ1) for 12 h prior to flow cytometry analysis of infected cells (n = 1,811 to 5,830). (B) Same as for panel A except that J774A.1 cells were infected with *M. marinum* strains expressing GFP.

kinetics of GFP expression upon addition and removal of preQ1 in both *M. smegmatis* and *M. marinum*, a fish and amphibian pathogen that is used as a model organism for *M. tuberculosis* (see Fig. S2 in the supplemental material). GFP repression upon addition of preQ1 and recovery following removal of preQ1 occurred within ca. 2 to 3 doubling times in both *M. smegmatis* and *M. marinum*, confirming the reversibility of the response. Further, flow cytometry on preQ1-treated *M. smegmatis* confirmed that the riboswitch is titratable (versus binary, as in the nitrile-inducible system [25]) and on average the entire cell population responds to a given dose of preQ1 (see Fig. S6 in the supplemental material). Finally, J774A.1 macrophage-like cells were infected with either *M. smegmatis* or *M. marinum* expressing GFP under the control of the *B. subtilis trans* riboswitch and treated with 1 mM or 100 μM preQ1 (Fig. 7). Flow cytometry revealed that both *M. smegmatis* and *M. marinum* within macrophages responded to preQ1, as demonstrated by a reduction in GFP fluorescence. PreQ1 at these concentrations was not toxic to mammalian cells (as determined by alamarBlue staining; data not shown) and did not affect bacterial load in infected macrophages over the time course of infection (see Fig. S7 in the supplemental material).

DISCUSSION

Overall, our results indicate that preQ1 is stable in culture over hours to days, enters into the cytosol of mycobacteria in *in vitro* culture and in infected macrophages,

accumulates at concentrations sufficient to activate preQ1 riboswitches, and induces a reversible response. By altering the conformational equilibrium between ON and OFF states by mutation and modulating the transcript expression levels, we successfully obtained a preQ1 riboswitch construct appropriate for inducible knockdown/knockout applications in mycobacteria. In addition to fulfilling our goals for riboswitches as tools, our characterization of rationally designed variants offered additional insights into preQ1 riboswitch mechanism and behavior, as discussed further below.

Among naturally occurring riboswitches, the diverse GFP expression levels observed in the absence of preQ1 could indicate that differences that are unrelated to the aptamer (e.g., RBS sequence and number of nucleotides between the RBS and the start codon) are independent factors that significantly influence observed expression levels, as has been previously suggested (26). Since the efflux pump inhibitors CCCP and reserpine did not influence the dose-dependent response to preQ1, active efflux is not a mechanism that appears to limit intracellular preQ1, and thus incomplete repression is probably not due to insufficient ligand. Instead, incomplete repression and the relatively low response ratios (<3) may indicate that naturally occurring preQ1 riboswitches have an inherently limited range and complete repression is not required for their physiological function or that, as a heterologous host, *M. smegmatis* lacks necessary additional factors or the appropriate intracellular milieu to recapitulate the native behavior of these riboswitches.

The thermodynamic parameters obtained for the wild-type and variant switches provide further information about the effects of mutation on riboswitch properties. For example, the significant difference between the observed K_{d1} for the *T. tencongensis* wild type and the value measured *in vitro* for the aptamer is striking (115 versus 2 to 7 nM) (Table 1) (17, 22). On the one hand, this could indicate that the intracellular preQ1 concentration is lower than the exogenously applied concentration at equilibrium for all concentrations tested. However, the discrepancy is specific to the *T. tencongensis* switch, since the K_{d1} values for the *B. subtilis trans* variant and the *L. rhamnosus* wild type ($\sim$10 to 15 nM) are within severalfold of the *in vitro* value (Table 1). In other words, for the *T. tencongensis* wild-type riboswitch the preQ1 concentration required to effect function and presumably preQ1 binding is much greater than the thermodynamic binding constant. This condition is a classic indication that the riboswitch is operating under kinetic rather than thermodynamic control (27, 28). In contrast, the apparent K_{d1} of the *T. tencongensis* variants is on the same order as the *in vitro* K_d for the aptamer (Table 1). These results could indicate that stabilizing P2 shifts the *T. tencongensis* riboswitch into a thermodynamic control regime, as has been suggested for the effect of stabilizing the sequester helix of the theophylline riboswitch (19). Consistent with this hypothesis, the K_{d1} among the *T. tencongensis* variants, which we predicted have more stable OFF states than the wild type, is relatively constant, and their behavior conforms qualitatively to thermodynamic predictions.

By the same reasoning, both the *B. subtilis trans* and *L. rhamnosus* riboswitches are thermodynamically controlled in mycobacteria, since the observed K_{d1} are commensurate with reported *in vitro* aptamer binding constants (Table 1). However, applying mutations to the corresponding P2 or P3 stem did not result in the expected behavioral trends in either riboswitch. Although the loss of preQ1 sensitivity for variants B1, B2, L1, and L3 may be the result of overstabilizing the OFF state (Fig. 4B and 5B), the high expression and low response ratio of variant L2 does not conform to this reasoning unless we assume that the additional inserted nucleotides that connect the loop to P2 (Fig. 5A) are significantly destabilizing. On the other hand, modification of the P4 stem in the L. rhamnosus riboswitch led to one variant, L4, that is comparable to T4 in its behavior, with an improved response ratio of $\sim$5 (versus $\sim$2.5 for the wild type).

Interestingly, the K_{int} values determined for the riboswitches and their variants (Table 1) were all close to 1 and indicate that the conformational states A and B are close in energy, a finding consistent with the high degree of similarity between the unliganded apo and preQ1-bound structures of the *T. tencongensis* riboswitch (17). However, the observed differences in free energy ($\Delta\Delta G$) between *T. tencongensis*

variants were not well predicted by mfold calculations (Table 1). In particular, the destabilization of variants T1 to T3 was significantly overestimated. Designing rational changes that introduce only the desired changes to the target thermodynamic parameters is a major challenge, as illustrated by the trends among the *T. tencongensis* variants and the unexpected behavior of the *L. rhamnosus* and *B. subtilis* variants. One potential strategy for more conservative mutations is to examine sequence variation in the expression platform across all riboswitches of a given class and type. This "evolutionary" approach has been applied to the FMN riboswitch to characterize how modulation of the P1 stem of the aptamer alters the ligand on and off rates and hence the dissociation constant, although only binding and not FMN-responsive function was assayed in this *in vitro* study (29).

Perhaps the most unexpected results were observations that support a second, lower-affinity preQ1 binding site. A second transition has not been noted in other studies that examined preQ1-aptamer binding *in vitro* (11, 15–17, 20–22, 30, 31). In most reports, however, preQ1 binding was only determined up to a maximum concentration of 100 μM preQ1. In a notable exception, McCown et al. presented in-line probing data up to 1 mM preQ1 for type I and type II riboswitches (11). Although these researchers report fits to a single equilibrium, their raw data indicate two independent binding equilibria with apparent dissociation constants around 0.1 and 100 μM. These *in vitro* binding data further support our interpretation that the additional preQ1-dependent transition we observe is inherent to the riboswitch and not an artifact of our live cell reporter system. Interestingly, variants B1, B2, and L2 all displayed insensitivity to preQ1 at low micromolar preQ1 but responses at high micromolar concentrations; this behavior was especially notable in L2 (Fig. 4C and D). The apparent loss of high-affinity binding with preservation of the lower-affinity interaction further supports the existence of two noncooperative binding sites. Also, in terms of inducible gene regulation in mycobacteria, the additional repression at 1 mM preQ1 affords a higher dynamic range for knockdown applications (see Fig. S8 in the supplemental material).

Only two other naturally occurring riboswitches are known to bind to two ligand molecules simultaneously: the glycine and tetrahydrofolate (THF) riboswitches (32–34). Although the glycine riboswitch is composed of two distinct aptamer domains, the THF riboswitch binds two ligands in a single domain. Unlike our observations of the preQ1 riboswitches, THF binding was shown to be strongly cooperative under physiological conditions, although intriguingly only one site is required to induce a regulatory response (34). In that study, Trausch et al. proposed that the second site may have evolved to provide a more digital response to THF or to simultaneously detect guanine. Since intracellular levels of preQ1 are not known, the physiological importance of riboswitch responses at concentrations 1,000-fold above the higher-affinity K_d is not clear. One intriguing possibility is that the additional, or "secondary," binding site is more specific for a related metabolite such as guanine, whose affinity for the primary binding site is several orders of magnitude weaker than that of preQ1 (15). Regardless, the phenomenon must be considered for both the engineering and application of preQ1 riboswitches as gene regulation tools since it clearly influences the overall behavior of the riboswitch, at least in mycobacteria. Further studies are needed into the molecular basis of the apparent additional binding event and its potential relevance in queuosine-synthesizing bacteria.

In addition to their utility as orthogonal gene regulation tools, riboswitches can also be used as cellular sensors. When the target ligand is an endogenous metabolite, a modified riboswitch may be necessary to provide sufficient sensitivity and dynamic range to detect changes in intracellular concentration. In the case of preQ1, for example, the reporter protein β-galactosidase is largely repressed in the host organism *B. subtilis* when regulated by wild-type versus destabilized mutant riboswitches (6, 15). Our *T. tencongensis* variants, which maintain responses over nM to μM preQ1 but have greater dynamic range, may be appropriate for sensing changes in intracellular preQ1 in bacteria that synthesize queuosine.

As shown by the riboswitch response and low toxicity of preQ1 in macrophages,

preQ1 riboswitches also show promise in infection models and in the future could be multiplexed with other regulatory methods like the Tet-inducible system (5) to provide time-dependent control over multiple genes simultaneously. This approach would permit, for example, two genes with redundant functions to be assayed for their relative contributions to bacterial virulence and survival over the course of infection. Recently, inducible gene knockdown has been demonstrated in mycobacteria using CRISPR interference (CRISPRi) methods (35, 36). Because gene targeting is achieved via the expression short gene-specific guide RNAs, this method offers a facile means of controlling different genes and, presumably, multiple targets simultaneously. As with protein repressor-based systems, additional machinery (in this case, the catalytically deficient endonuclease dCas9) must be stably coexpressed and potential off-target effects have yet to be assessed. Since each approach to mycobacterial gene regulation has its pros and cons, a diverse toolbox is required to meet varied needs. The optimization and characterization presented here informs the application of engineered preQ1 riboswitch-based tools, as well as our understanding of native preQ1 riboswitches.

MATERIALS AND METHODS

Cell strains and culture conditions. Unless otherwise noted, *Mycobacterium smegmatis* mc^{2}155 (ATCC 700084) was cultured on Middlebrook 7H11 agar (BD) or Middlebrook 7H9 liquid (BD) medium with 10% ADC supplement (BD), 0.5% (vol/vol) glycerol, and 0.05% (vol/vol) Tween 80. *E. coli* Stellar cells (Clontech) were cultured on LB agar or liquid medium with 50 μg/ml kanamycin. *M. smegmatis* was incubated at 37°C and, for liquid cultures, at 225 rpm. *Mycobacterium marinum* M (ATCC BAA-535) was cultured on 7H11 agar or 7H9 liquid medium with 10% oleic acid-albumin-dextrose-catalase (OADC) supplement (BD), 0.5% glycerol, and 25 μg/ml kanamycin. *M. marinum* cultures were grown at 30°C in the dark; for liquid cultures, the medium also contained 0.05% Tween 80 and were shaken at 110 rpm. Where applicable, plasmids were selected with kanamycin at 50 μg/ml in *E. coli* and 25 μg/ml in mycobacteria and hygromycin at 100 μg/ml in *E. coli* and 20 μg/ml in mycobacteria. When selecting for double transformants, 12.5 μg/ml kanamycin and 25 μg/ml hygromycin were used. The J774A.1 monocyte-derived cell line (ATCC TIB-67) was cultured in Dulbecco modified Eagle medium (DMEM) with 10% fetal bovine serum and glucose at 4.5 g/liter unless otherwise noted.

Construction of riboswitch-controlled GFP reporter constructs. Riboswitch-controlled reporter constructs were generated by modification of the GFP reporter plasmid pMWS114 (4) by three methods: cloning of an insert generated with assembly PCR, cloning of an insert generated by nested primer PCR, or by site-directed mutagenesis (see Table S1 in the supplemental material). PCR products comprised the *hsp60* promoter (P_{hsp60}) (14) with the riboswitch sequence inserted at the 3′ end by assembly or nested primers. Inserts were cloned into pMWS114 via the KpnI and BamHI sites by ligation or the XbaI and MscI sites by In-Fusion cloning (Clontech). For TetR-controlled GFP expression, the *egfp* gene was amplified from pMWS114 and inserted via the PacI and EcoRV sites into pTet-GW (a gift from Christopher Sassetti), which contains the tetracycline-inducible promoter pUV15tetO (37). Sequence-verified constructs were electroporated (1,000 Ω, 25 μF, and 2.5 kV) into *M. smegmatis* and transformants selected on 7H11 agar with kanamycin at 37°C for 3 days. Cell stocks were made from single colonies inoculated into 7H9 medium with kanamycin and grown to an optical density at 600 nm (OD_{600}) of ~1 at 37°C with shaking at 250 rpm.

GFP fluorescence endpoint assay. PreQ1 (Chem-Master International, Inc., and a gift from Dirk Iwata-Reuyl) was synthesized as described previously (15), dissolved in DMSO, and serially diluted to generate 100-fold-concentrated stock solutions. The fluorescence assay was performed largely as described previously (23). Briefly, starter cultures of *M. smegmatis* were grown overnight to OD_{595} of ~1 and subcultured at OD_{595} of 0.2 in 1 ml of 7H9 medium containing preQ1. The final concentration of DMSO in all samples was 1%. After incubation at 37°C and 250 rpm for 6 h (~2 doubling times), 200 μl of culture per sample was divided into aliquots in black, clear-bottom 96-well plates (Costar). Fluorescence was recorded with an F5 Filtermax plate reader (Molecular Devices) using 485-nm excitation and 535-nm emission filters. The OD_{595} was measured in parallel and used to normalize GFP fluorescence values.

RNA free energy calculations. All free energy calculations were performed with the RNA folding form on the mfold server using default parameters (http://unafold.rna.albany.edu) (18). Because the complex tertiary pseudoknot structures of the preQ1 riboswitches are not predicted by the mfold algorithm, calculations were performed on only the P2 stem of the *T. tencongensis* and *B. subtilis* riboswitches and the P3 stem of the *L. rhamnosus* riboswitch. The input sequence comprised the two halves of the stem sequence connected by a 6-nt poly(A) (A_6) linker. The linker was chosen not to interact with the P2 sequence and to be sufficiently long to avoid adding additional strain upon stem formation. Calculations were performed the same way for the *L. rhamnosus* P4 stem, except that this stem did not require a linker.

Equilibrium modeling of ligand-dependent riboswitch responses. For the complete derivation of the two-state model with one or two independent binding sites, see the supplemental material. Briefly, it was assumed that the riboswitch response is dominated by the equilibrium between an ON state (A) and an OFF state (B) that is described by an "intrinsic" equilibrium constant K_{int} (Fig. 3A, scheme 1). For

the preQ1 riboswitch, which is a ligand-responsive OFF switch, ligand (L) is assumed to bind only to B, and in the model with two binding sites (Fig. 3A, scheme 2), L can bind at either of two independent binding sites in B with corresponding dissociation constants K_{d1} and K_{d2}. The observed riboswitch response (as assessed by protein expression) is determined by the relative protein concentration, $[P]_{rel}$, and is proportional to the ratio of transcripts in the ON state over the total number of transcripts. By the steady-state assumption, $[P]_{rel}$ reduces to an expression dependent on the concentration of ligand L and the equilibrium constants K_{int} and K_d (or, for two independent binding sites, K_{d1} and K_{d2}). For the fits shown in Fig. 4, fluorescence data from all biological and technical replicates for each series were fit to equation S12 in the supplemental material using KaleidaGraph (Synergy Software).

Construction of integrating riboswitch-controlled GFP and LprG constructs. Riboswitch-controlled GFP reporter and positive-control constructs were generated by digesting the appropriate episomal constructs (pMWS114, pEV06, pEV13, and pEV12 [see Table S1 in the supplemental material]) with XbaI and HindIII to excise the promoter, riboswitch, and *egfp* gene as a continuous insert. Each resulting fragment was ligated into the integrating vector pMV306 to generate the corresponding integrating construct (pEV40-43 [see Table S1 in the supplemental material]) (14). To create a construct expressing LprG under riboswitch control, pEV43 was modified via site-directed mutagenesis to introduce an NdeI restriction site between the riboswitch and *egfp*. The *egfp* gene was removed via the NdeI and HindIII sites and replaced with the *lprG* gene from *M. smegmatis* (MSMEG_3070; amplified as a C-terminally 3×FLAG-tagged fusion) by In-Fusion cloning (Clontech) to generate pEV46. Sequence-verified constructs were transformed into *M. smegmatis*, selected, and propagated as described above.

Immunoblot endpoint assay for GFP and LprG. *M. smegmatis* strains harboring a single chromosomally integrated copy of *egfp* controlled by a constitutive promoter or preQ1 riboswitch variants (pEV40-43 [see Table S1 in the supplemental material]) were grown overnight to an OD_{595} of ~1 and subcultured at an OD_{595} of 0.2 in 10 ml of 7H9 medium containing preQ1. The final concentration of DMSO in all samples was 1%. After incubation at 37°C and 250 rpm for 6 h, the cells were pelleted, resuspended in 1 ml of PBS with 0.05% Tween 80, and lysed by sonication. Cleared total lysates were normalized to the absorbance at 280 nm, run on reducing SDS-PAGE, transferred to nitrocellulose membranes (0.45 μm; Bio-Rad), and probed with mouse anti-GFP (1:10,000; Invitrogen) and mouse anti-GroEL (1:5,000; Abcam) for 1 h with agitation at room temperature. After washing, membranes were probed with secondary antibody goat anti-mouse 800CW (1:15,000; LI-COR). Immunoblots were visualized using an Odyssey CLx infrared imager (LI-COR).

Immunoblot analysis of LprG was performed as described above, with the following exceptions. *M. smegmatis* harboring LprG-expressing integrating constructs was incubated with preQ1 for 6 h or 18 h prior to harvesting and analysis. Blots were probed with mouse anti-FLAG (1:1,000; clone M2, Sigma-Aldrich) and mouse anti-GroEL (1:5,000; Abcam). After washing, membranes were probed with the secondary antibody goat anti-mouse IgG–horseradish peroxidase (1:10,000; Abcam). Immunoblots were visualized by chemiluminescence (Immobilon Western Chemiluminescent HRP Substrate; Millipore).

Construction and characterization of *M. smegmatis* with *katG* under riboswitch control. A homologous recombinant *M. smegmatis* strain with the chromosomal *katG* gene under the control of the T4 riboswitch was generated essentially as described previously (4). The pRiboS-*katG* suicide plasmid was modified to replace the theophylline riboswitch sequence with the T4 riboswitch sequence (see Table S1 in the supplemental material). After electroporation into *M. smegmatis*, kanamycin-resistant clones were selected, and a positive clone was validated by PCR. The half-maximum effective concentration of isoniazid (EC_{50}) for the resulting strain RiboS-*katG* was determined in a growth assay. Briefly, *M. smegmatis* was inoculated at OD 0.02 or 0.05 into 7H9 medium containing DMSO vehicle or 0.1 or 1 mM preQ1 and culture for 24 h before measuring the OD_{595}. Isoniazid dose-response curves were fit for the half-maximal effective concentration (EC_{50}) using Kaleidagraph (Synergy Software).

Flow cytometry of *M. marinum*-infected macrophages. *M. marinum* was transformed by electroporation with pST194 and selected on 7H11 agar for 4 to 6 days. Single colonies were inoculated into 7H9 medium and incubated for 3 days. *M. marinum* cells were washed twice with an equal volume of PBS and allowed to settle for 5 min to remove cell clumps before measuring the OD_{600}. A final suspension equivalent to an MOI of 5 (OD_{600} of $1 = 3 \times 10^8$ CFU) in 1 ml of DMEM was added to J774A.1 macrophage-like cells (ATCC TIB-67) seeded at 2×10^5 cells per well in a 12-well plate. After incubation at 30°C and 5% CO_2 for 1 h, infected macrophages were washed twice with 1 ml of PBS. After incubating macrophages in fresh DMEM containing amikacin for an additional 2 h to kill extracellular bacteria and repeating the PBS wash, infected monolayers were incubated in DMEM containing 0 or 100 μM preQ1 for a further 24 h. After repeating the PBS wash, the cells were fixed in 1 ml 4% paraformaldehyde in PBS for 30 min before scraping the cells into the buffer. The resulting cell suspensions were subjected to flow cytometry (Becton Dickinson FACScan; Flow Cytometry Laboratory, Stony Brook University) as reported (4) and analyzed using Cyflogic software (CyFlo, Ltd., Finland).

Flow cytometry of *M. smegmatis*-infected macrophages. *M. smegmatis* was cotransformed by electroporation with pMV306-mCherry and pMV261, pMWS114, pST194, or pEVV12 and selected on 7H11 agar for 3 days. Single colonies were inoculated into 7H9 medium and incubated overnight. *M. smegmatis* cells were washed twice with an equal volume of PBS before measuring the OD_{600}. A final suspension equivalent to an MOI of 10 (OD_{600} of $1 = 3 \times 10^8$ CFU) in 1 ml DMEM was added to J774A.1 macrophage-like cells seeded at 2×10^5 to 4×10^5 cells per well in a 12-well plate. Infection, washing, and preQ1 treatment were carried out as with *M. marinum* infection experiments, except that no amikacin treatment was applied. Instead, kanamycin at 5 μg/ml was added to maintain the episomal plasmids over the several *M. smegmatis* division cycles of the 12-h incubation (38). Cells were fixed after 12 h of preQ1 treatment, and the resulting cell suspensions were subjected to flow cytometry (LSRFortressa; Flow Cytometry Labora-

tory, Stony Brook University) and analyzed with Cyflogic software. Uninfected macrophages subjected to the same incubation protocol were used as a negative control to gate for mCherry-positive macrophages, which were further analyzed for mCherry and GFP fluorescence.

SUPPLEMENTAL MATERIAL

Supplemental material for this article may be found at https://doi.org/10.1128/JB.00656-16.

TEXT S1, PDF file, 0.7 MB.

ACKNOWLEDGMENTS

We thank Mary Lou Previti for assistance with cloning and Dirk Iwata-Reuyl, Hiren Patel, and members of the Seeliger lab for preliminary studies, helpful discussions, and critical reading of the manuscript.

This study was supported by National Institutes of Health 1R21AI103321 to J.C.S.

REFERENCES

1. Berens C, Suess B. 2015. Riboswitch engineering: making the all-important second and third steps. Curr Opin Biotechnol 31:10–15. https://doi.org/10.1016/j.copbio.2014.07.014.
2. Topp S, Reynoso CM, Seeliger JC, Goldlust IS, Desai SK, Murat D, Shen A, Puri AW, Komeili A, Bertozzi CR, Scott JR, Gallivan JP. 2010. Synthetic riboswitches that induce gene expression in diverse bacterial species. Appl Environ Microbiol 76:7881–7884. https://doi.org/10.1128/AEM.01537-10.
3. Reynoso CM, Miller MA, Bina JE, Gallivan JP, Weiss DS. 2012. Riboswitches for intracellular study of genes involved in *Francisella* pathogenesis. mBio 3:e00253-12. https://doi.org/10.1128/mBio.00253-12.
4. Seeliger JC, Topp S, Sogi KM, Previti ML, Gallivan JP, Bertozzi CR. 2012. A riboswitch-based inducible gene expression system for mycobacteria. PLoS One 7:e29266. https://doi.org/10.1371/journal.pone.0029266.
5. Gandotra S, Schnappinger D, Monteleone M, Hillen W, Ehrt S. 2007. *In vivo* gene silencing identifies the *Mycobacterium tuberculosis* proteasome as essential for the bacteria to persist in mice. Nat Med 13:1515–1520. https://doi.org/10.1038/nm1683.
6. Wu MC, Lowe PT, Robinson CJ, Vincent HA, Dixon N, Leigh J, Micklefield J. 2015. Rational re-engineering of a transcriptional silencing preQ1 riboswitch. J Am Chem Soc 137:9015–9021. https://doi.org/10.1021/jacs.5b03405.
7. Robinson CJ, Vincent HA, Wu MC, Lowe PT, Dunstan MS, Leys D, Micklefield J. 2014. Modular riboswitch toolsets for synthetic genetic control in diverse bacterial species. J Am Chem Soc 136:10615–10624. https://doi.org/10.1021/ja502873j.
8. Dixon N, Robinson CJ, Geerlings T, Duncan JN, Drummond SP, Micklefield J. 2012. Orthogonal riboswitches for tuneable coexpression in bacteria. Angew Chem Int Ed Engl 51:3620–3624. https://doi.org/10.1002/anie.201109106.
9. Dixon N, Duncan JN, Geerlings T, Dunstan MS, McCarthy JE, Leys D, Micklefield J. 2010. Reengineering orthogonally selective riboswitches. Proc Natl Acad Sci U S A 107:2830–2835. https://doi.org/10.1073/pnas.0911209107.
10. Urbonavicius J, Qian Q, Durand JM, Hagervall TG, Bjork GR. 2001. Improvement of reading frame maintenance is a common function for several tRNA modifications. EMBO J 20:4863–4873. https://doi.org/10.1093/emboj/20.17.4863.
11. McCown PJ, Liang JJ, Weinberg Z, Breaker RR. 2014. Structural, functional, and taxonomic diversity of three PreQ1 riboswitch classes. Chem Biol 21:880–889. https://doi.org/10.1016/j.chembiol.2014.05.015.
12. Eichhorn CD, Kang M, Feigon J. 2014. Structure and function of preQ1 riboswitches. Biochim Biophys Acta 1839:939–950. https://doi.org/10.1016/j.bbagrm.2014.04.019.
13. McCarty RM, Somogyi A, Lin G, Jacobsen NE, Bandarian V. 2009. The deazapurine biosynthetic pathway revealed: in vitro enzymatic synthesis of PreQ(0) from guanosine 5′-triphosphate in four steps. Biochemistry 48:3847–3852. https://doi.org/10.1021/bi900400e.
14. Stover CK, de la Cruz VF, Fuerst TR, Burlein JE, Benson LA, Bennett LT, Bansal GP, Young JF, Lee MH, Hatfull GF, et al. 1991. New use of BCG for recombinant vaccines. Nature 351:456–460. https://doi.org/10.1038/351456a0.
15. Roth A, Winkler WC, Regulski EE, Lee BW, Lim J, Jona I, Barrick JE, Ritwik A, Kim JN, Welz R, Iwata-Reuyl D, Breaker RR. 2007. A riboswitch selective for the queuosine precursor preQ1 contains an unusually small aptamer domain. Nat Struct Mol Biol 14:308–317. https://doi.org/10.1038/nsmb1224.
16. Meyer MM, Roth A, Chervin SM, Garcia GA, Breaker RR. 2008. Confirmation of a second natural preQ1 aptamer class in *Streptococcaceae* bacteria. RNA 14:685–695. https://doi.org/10.1261/rna.937308.
17. Jenkins JL, Krucinska J, McCarty RM, Bandarian V, Wedekind JE. 2011. Comparison of a preQ1 riboswitch aptamer in metabolite-bound and free states with implications for gene regulation. J Biol Chem 286:24626–24637. https://doi.org/10.1074/jbc.M111.230375.
18. Zuker M. 2003. Mfold web server for Nucleic acid folding and hybridization prediction. Nucleic Acids Res 31:3406–3415. https://doi.org/10.1093/nar/gkg595.
19. Mishler DM, Gallivan JP. 2014. A family of synthetic riboswitches adopts a kinetic trapping mechanism. Nucleic Acids Res 42:6753–6761. https://doi.org/10.1093/nar/gku262.
20. Liberman JA, Salim M, Krucinska J, Wedekind JE. 2013. Structure of a class II preQ1 riboswitch reveals ligand recognition by a new fold. Nat Chem Biol 9:353–355. https://doi.org/10.1038/nchembio.1231.
21. Kang M, Eichhorn CD, Feigon J. 2014. Structural determinants for ligand capture by a class II preQ1 riboswitch. Proc Natl Acad Sci U S A 111:E663–E671. https://doi.org/10.1073/pnas.1400126111.
22. Suddala KC, Rinaldi AJ, Feng J, Mustoe AM, Eichhorn CD, Liberman JA, Wedekind JE, Al-Hashimi HM, Brooks CL, III, Walter NG. 2013. Single transcriptional and translational preQ1 riboswitches adopt similar prefolded ensembles that follow distinct folding pathways into the same ligand-bound structure. Nucleic Acids Res 41:10462-75. https://doi.org/10.1093/nar/gkt798.
23. Van Vlack ER, Seeliger JC. 2015. Using riboswitches to regulate gene expression and define gene function in mycobacteria. Methods Enzymol 550:251–265. https://doi.org/10.1016/bs.mie.2014.10.034.
24. Ranes MG, Rauzier J, Lagranderie M, Gheorghiu M, Gicquel B. 1990. Functional analysis of pAL5000, a plasmid from *Mycobacterium fortuitum*: construction of a "mini" mycobacterium-*Escherichia coli* shuttle vector. J Bacteriol 172:2793–2797. https://doi.org/10.1128/jb.172.5.2793-2797.1990.
25. Pandey AK, Raman S, Proff R, Joshi S, Kang C-M, Rubin EJ, Husson RN, Sassetti CM. 2009. Nitrile-inducible gene expression in mycobacteria. Tuberculosis 89:12–16. https://doi.org/10.1016/j.tube.2008.07.007.
26. Gold L. 1988. Posttranscriptional regulatory mechanisms in *Escherichia coli*. Annu Rev Biochem 57:199–233. https://doi.org/10.1146/annurev.bi.57.070188.001215.
27. Wickiser JK, Cheah MT, Breaker RR, Crothers DM. 2005. The kinetics of ligand binding by an adenine-sensing riboswitch. Biochemistry 44:13404–13414. https://doi.org/10.1021/bi051008u.
28. Wickiser JK, Winkler WC, Breaker RR, Crothers DM. 2005. The speed of RNA transcription and metabolite binding kinetics operate an FMN riboswitch. Mol Cell 18:49–60. https://doi.org/10.1016/j.molcel.2005.02.032.
29. Rode AB, Endoh T, Sugimoto N. 2015. Tuning riboswitch-mediated gene regulation by rational control of aptamer ligand binding properties.

Angew Chem Int Ed Engl 54:905–909. https://doi.org/10.1002/anie.201407385.
30. Klein DJ, Edwards TE, Ferre-D'Amare AR. 2009. Cocrystal structure of a class I preQ1 riboswitch reveals a pseudoknot recognizing an essential hypermodified nucleobase. Nat Struct Mol Biol 16:343–344. https://doi.org/10.1038/nsmb.1563.
31. Rieder U, Kreutz C, Micura R. 2010. Folding of a transcriptionally acting preQ1 riboswitch. Proc Natl Acad Sci U S A 107:10804–10809. https://doi.org/10.1073/pnas.0914925107.
32. Butler EB, Xiong Y, Wang J, Strobel SA. 2011. Structural basis of cooperative ligand binding by the glycine riboswitch. Chem Biol 18:293–298. https://doi.org/10.1016/j.chembiol.2011.01.013.
33. Mandal M, Lee M, Barrick JE, Weinberg Z, Emilsson GM, Ruzzo WL, Breaker RR. 2004. A glycine-dependent riboswitch that uses cooperative binding to control gene expression. Science 306:275–279. https://doi.org/10.1126/science.1100829.
34. Trausch JJ, Ceres P, Reyes FE, Batey RT. 2011. The structure of a tetrahydrofolate-sensing riboswitch reveals two ligand binding sites in a single aptamer. Structure 19:1413–1423. https://doi.org/10.1016/j.str.2011.06.019.
35. Singh AK, Carette X, Potluri LP, Sharp JD, Xu R, Prisic S, Husson RN. 2016. Investigating essential gene function in *Mycobacterium tuberculosis* using an efficient CRISPR interference system. Nucleic Acids Res 44:e143. https://doi.org/10.1093/nar/gkw625.
36. Choudhary E, Thakur P, Pareek M, Agarwal N. 2015. Gene silencing by CRISPR interference in mycobacteria. Nat Commun 6:6267. https://doi.org/10.1038/ncomms7267.
37. Ehrt S, Guo XV, Hickey CM, Ryou M, Monteleone M, Riley LW, Schnappinger D. 2005. Controlling gene expression in mycobacteria with anhydrotetracycline and Tet repressor. Nucleic Acids Res 33:e21. https://doi.org/10.1093/nar/gni013.
38. Srivastava V, Rouanet C, Srivastava R, Ramalingam B, Locht C, Srivastava BS. 2007. Macrophage-specific *Mycobacterium tuberculosis* genes: identification by green fluorescent protein and kanamycin resistance selection. Microbiology 153:659–666. https://doi.org/10.1099/mic.0.2006/000547-0.